01 Aug 2005

Autoionization of He Atoms by Partially Stripped Ion Impact

Sebastian Otranto
Missouri University of Science and Technology, otrantos@mst.edu

Ronald E. Olson
Missouri University of Science and Technology, olson@mst.edu

Recommended Citation

S. Otranto and R. E. Olson, "Autoionization of He Atoms by Partially Stripped Ion Impact," *Physical Review A*, American Physical Society (APS), Aug 2005.
The definitive version is available at https://doi.org/10.1103/PhysRevA.72.022716

Autoionization of He atoms by partially stripped ion impact

S. Otranto* and R. E. Olson
Physics Department, University of Missouri–Rolla, Rolla, Missouri 65401, USA
(Received 5 May 2005; published 17 August 2005)

A study of the autoionization process induced by partially stripped ion impact is performed. Electron spectra in momentum space are predicted within a classical model for partially stripped ions. The results are compared with those obtained for pure Coulomb-like projectiles. A quantum-mechanical extension of the Barrachina-Macek model is proposed for partially stripped projectiles. Structure on the electron angular distribution arising in quantum and classical treatments is identified and compared. The presence of rainbow scattering interference is observed in the binary ring profile of the outgoing autoionized electrons for positive-ion impact.

DOI: 10.1103/PhysRevA.72.022716 PACS number(s): 34.50.Fa

I. INTRODUCTION

One of the processes observed during the collision of charged particles and photons with atoms is the ionization of a single electron, leaving the target with one extra unit of positive charge. Two main mechanisms underlie this process: direct single ionization and the two-step Auger effect. For the latter, during the collision the incident particle (or photon) leaves the target atom in an excited state which then decays in a radiationless transition where one electron is emitted to the continuum. When a two-electron atom is involved, so that the intermediate state is doubly excited, the process is known as autoionization. Usually, the term Auger effect is reserved for electron emission produced after an inner-shell vacancy is created in a many-electron atom, the name given to honor the discovery of Auger in 1925 [1]. The electron emission is a consequence of the rearrangement of the atom after an inner-shell vacancy produces an unstable continuum level.

Autoionization induced by ion impact can give rise to electron spectra different from those produced by photons. In the former, the electrons are emitted not only in the presence of the residual target but also in that of the projectile ion. Thus, the energy and angular distribution of the ionized electrons are distorted by the presence of the projectile and differ from the isotropic behavior typical of those produced by photon impact. For ion impact one observes a shift in the electron emission energy due to the electron being created in the fields of both the projectile and target ions. This produces an asymmetrical profile which contrasts with a typical isotropic Lorentzian pattern. Such effects were discussed in a pioneering paper by Barker and Berry in 1966 who employed a classical model [2]. For more than a decade, their model was used to describe autoionization following ion impact. In 1977, Devdariani *et al.* developed the first quantum-mechanical model [3] that used the same assumptions as those of Barker and Berry, albeit in a quantal format. They assumed that the projectile distorted the electron's energy but not its trajectory. More recently, van der Straten and Morgenstern employed the eikonal model in order to introduce the postcollisional interaction (PCI) between the emitted electron and the projectile [4]. In 1989, Barrachina and Macek [5] successfully developed a continuum-distorted-wave (CDW) theory that predicted Coulomb focusing during the PCI between projectile and autoionized electron. Their predictions were experimentally verified the same year by Swenson *et al.* [6]. This model with its subsequent improvements [7–9] account for the Stark effect (which is very important when the impinging ion energy is rather low) and the modification of the intermediate excited-state lifetime due to the transient presence of the projectile.

Meanwhile, the classical description of the process was not forgotten. In 1989 and 1991 Swenson *et al.* used a Coulomb path interference mechanism in order to give a classical description to the Coulomb focusing mechanism [6,10]. The authors concluded that this process is a consequence of the electrons being emitted in the forward direction at slightly different emission times so that the electrons follow different paths, but asymptotically have the same velocity. The Coulomb path interference thus represents an ion-atom collision analog to the classical double-slit electron mechanism.

Using semiclassical analysis, the interference structures predicted in the CDW spectral lines have been interpreted in terms of a *nearside-farside* scattering, which was first used to describe elastic reactions of spin-zero nuclei [11]. Here, the autoionization amplitude is composed of two terms which are related to electron trajectories that have both positive and negative deflection angles. Kunikeev and Senashenko [12] interpreted oscillatory structures in the resonant lines as an interference between waves that are, and are not, scattered by the projectile.

All the above-mentioned analysis considered Coulomb-like fully stripped projectiles. However, it is known that partially stripped ions show more complex collision dynamics in single-ionizing collisions. Oscillations in the emitted electron spectrum in the region of the binary peak have been experimentally observed and theoretically reproduced [13,14]. These oscillations have been attributed to interference structure in the elastic differential cross section for the scattering of target electrons from the impinging ion. Furthermore, this phenomenon has been associated with the well-known rainbow scattering [15].

In this work, we concentrate on the autoionization of atoms by partially stripped ion impact. We perform a simula-

*Email: otrantos@umr.edu On leave from Dto. de Física, Universidad Nacional del Sur, 8000 Bahía Blanca, Argentina

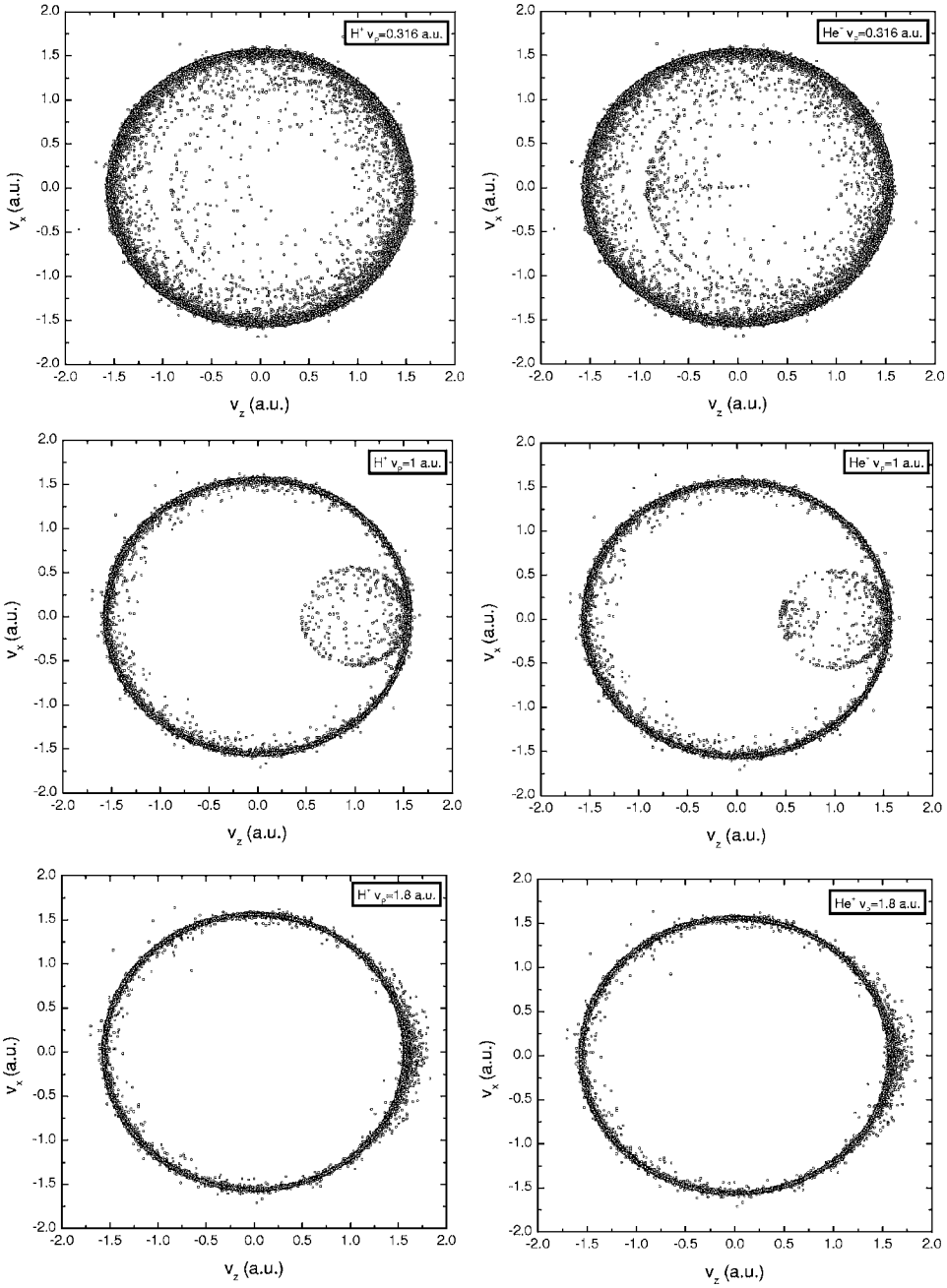

FIG. 1. Electron distribution in velocity space for the $2s^2(^1S)$ autoionizing state of He. Left column, H^+ projectiles. Right column, He^+ projectiles. The impact velocity for each row is (a) 0.316, (b) 1, and (c) 1.8 a.u.

tion of the autoionization process in classical terms and obtain electron spectra that we display in velocity space. Histograms for the binary ring profile are presented for different impinging ions and the observed structures are compared with those present in the classical and quantum-mechanical elastic differential cross sections for a parallel incident beam. An extension of the Barrachina-Macek model is proposed in order to give a quantum-mechanical description of the process and the results are compared with the classical simulation. The autoionization ring profile is obtained and differences among theories are explained. Finally, general conclusions are drawn.

Atomic units are used throughout this work unless explicitly stated otherwise.

II. THE CLASSICAL MODEL

In this section we describe the main features corresponding to our classical simulation of the autoionization process [16]. Let us consider the autoionization of an atom induced by ion impact. We assume that the projectile leaves the atom in a doubly excited state. Within the PCI scheme the atom spontaneously decays in the presence of the projectile. Thus, once the electron has been emitted by the atom, it also evolves under the influence of the projectile field. The dynamics of the electron can be best analyzed in a projectile reference system. In the PCI scheme the time-dependent problem of an electron evolving in two centers reduces to a time-independent problem of one electron in the field of only one center (the projectile). The time dependence leads to a

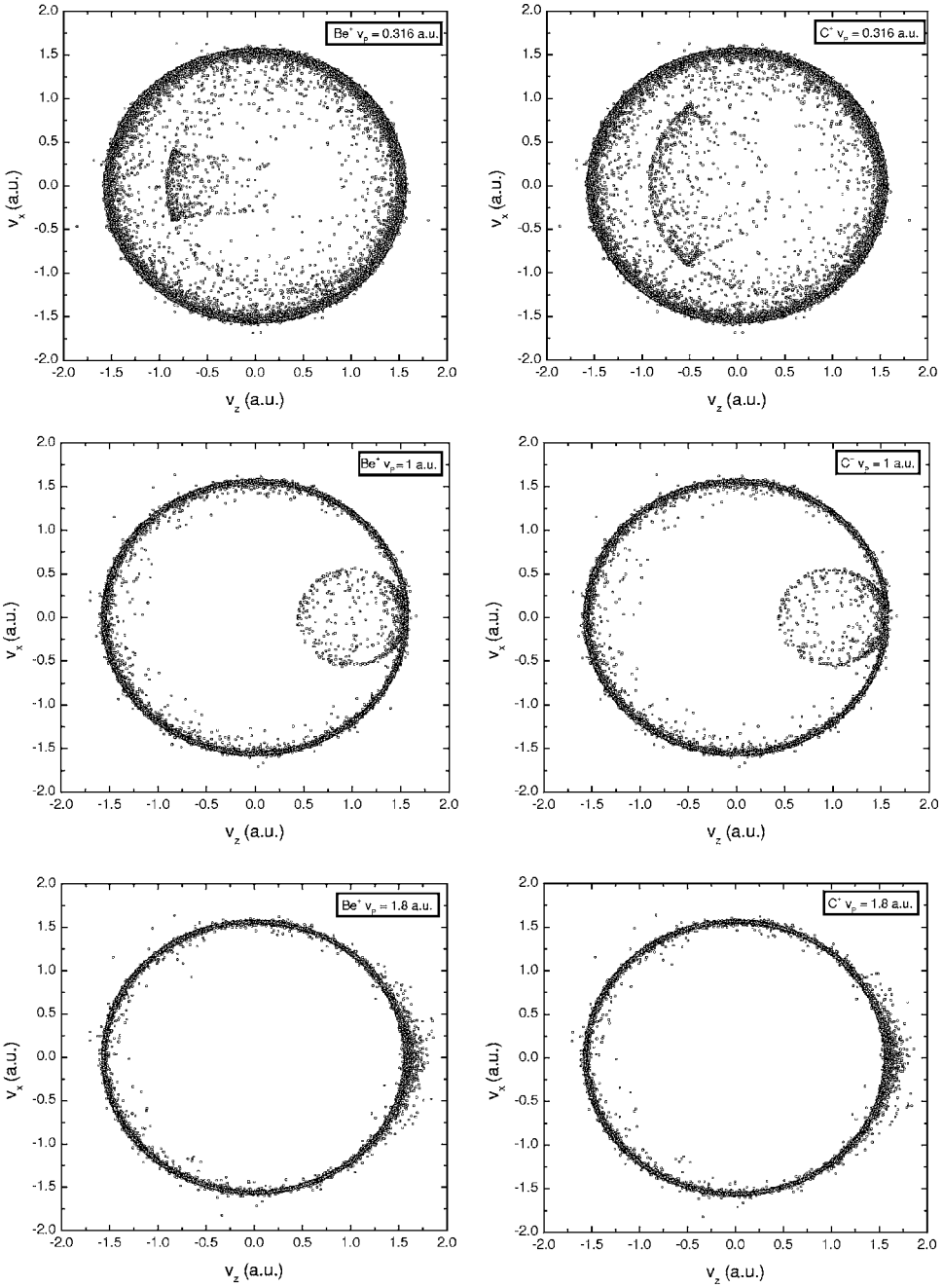

FIG. 2. Electron distribution in velocity space for the $2s^2(^1S)$ autoionizing state of He. Left column, Be^+ projectiles. Right column, C^+ projectiles. The impact velocity for each row is (a) 0.316, (b) 1, and (c) 1.8 a.u.

time-dependent initial condition for each of the electrons emitted by the autoionizing atom.

We study the trajectories of emitted electrons which interact only with the projectile field. This approximation is a considerable simplification but allows for an exact treatment of the problem. The initial conditions of the problem are given by defining the initial distance r_0 of the emitted electrons to the projectile and the emission velocity vector $\mathbf{v}_0$, while the incidence direction will be denoted as z. The velocity of the projectile is $\mathbf{v}_P$. Placing the reference system on the projectile, the energy balance reads

$$\frac{1}{2}mv^2 = \frac{1}{2}m\mathbf{v}_{emis}^2 + V_P(r_0) = E_0, \tag{1}$$

where $\mathbf{v}_{emis}$ represents the relative velocity of the emitted electron to the moving projectile and it is defined by $\mathbf{v}_{emis} = \mathbf{v}_0 - \mathbf{v}_P$ and v is the relative asymptotic velocity. The potential $V_P(r_0)$ is the projectile-emitted electron potential. For a partially stripped ion, the form of the potential is one that is parametrized in such a way that a large range of ionic species may be easily considered. We use the Hartree-Fock model potential of Garvey *et al.* [17] which simulates the

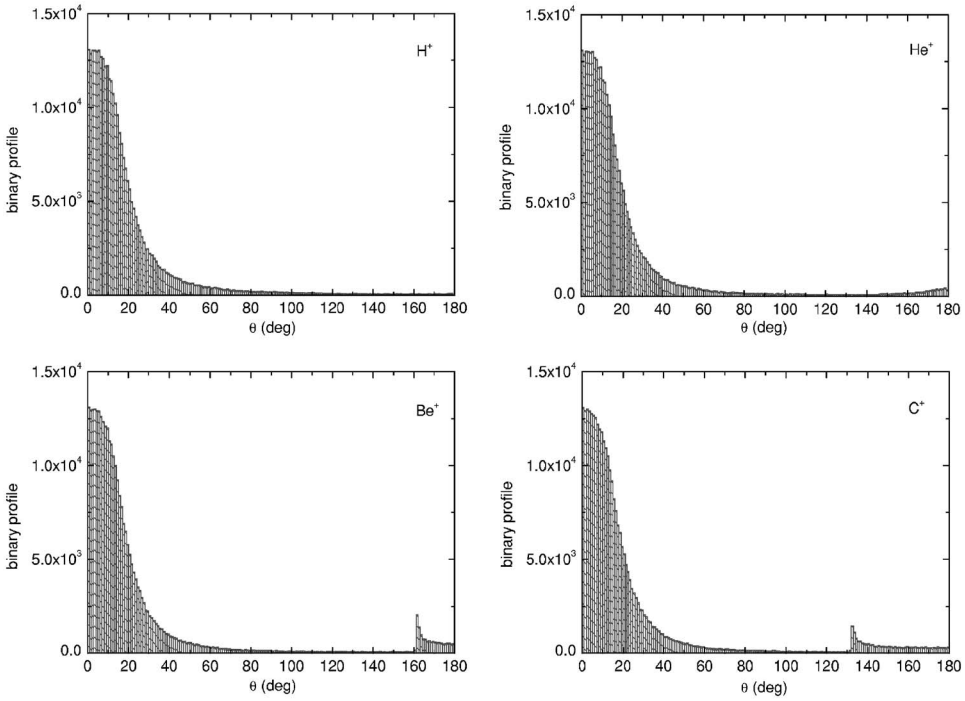

FIG. 3. Binary ring histograms using the classical model for the $2s^2(^1S)$ autoionizing state of He. The projectile velocity is $v_P = 0.316$ a.u.

interparticle-separation-dependent screening of the ion nuclear charge experienced by the electron and is given by

$$V_P(r) = \frac{\{(N-1)[1-\Omega(r)]-Z\}}{r},$$

$$\Omega(r) = \left[\left(\frac{\eta}{\xi}\right)(e^{\xi r}-1)+1\right]^{-1}. \tag{2}$$

Here, $(N-1)$ is the number of electrons present in the ion and η and ξ are the screening parameters which have been tabulated for ions $2 \leqslant Z \leqslant 54$. For heavier ions, the parameters may be found by a fit that utilizes points for a reduced parameter form of this potential [18].

We consider the trajectory of each emitted electron and evaluate its asymptotic velocity. By taking a large number of trajectories we compose the electron distribution in momentum space corresponding to the autoionization process. Until now we have made no assumption about the way in which the electrons are emitted. According to quantum theory [19], if the autoionization process takes place due to excitation of the ground state to an autoionizing state by photon absorption, the unperturbed electron intensity profile I is given by the Lorentzian

$$I = \frac{\Gamma^2}{\Gamma^2 + \frac{1}{4}(v_e^2 - \tilde{v}_0^2)^2} \tag{3}$$

where Γ is the full width at half maximum of the Lorentzian. We use this velocity profile to sort the initial electron velocity v_0 according to a Lorentzian distribution,

$$v_0 = \left[\tilde{v}_0^2 \pm 2\Gamma\left(\frac{1}{x}-1\right)^{1/2}\right]^{1/2} \tag{4}$$

with x a real number between 0 and 1. The velocity $\tilde{v}_0$ is the velocity acquired by the emitted electron while the other excited electron decays. For the He atom and for the autoionizing states $2s^2(^1S)$, $2p^2(^1D)$, and $2s2p(^1P)$ the values for Γ we used are 0.005 07, 0.002 65, and 0.0014 a.u. and their corresponding electron velocities $\tilde{v}_0$ are 1.5646, 1.6106, and 1.6168 a.u. [7].

According to Barker and Berry, the probability that the electron has been emitted at time t after the excitation has occurred is given by

$$P_{BB}(t) = 1 - e^{-\Gamma t}. \tag{5}$$

We use this relationship to weight the electron emission at different distances of the projectile. Letting y be a random variable uniformly distributed between 0 and 1, and since $t = r_0/v_P$, we obtain the following distribution for the initial position of the projectile:

$$r_0 = \frac{v_P}{\Gamma}|\ln(1-y)|. \tag{6}$$

For Coulomb-like projectiles use can be made of the Kepler equation and the Laplace-Runge-Lenz vector in order to obtain the asymptotic angle Θ for a given emission velocity $\mathbf{v}_0$ [16]. However, for partially stripped ions (or any other central potential), we have to make use of the relation between the polar angle and the orbit radius. The distance of closest approach will be denoted by r_{min} and can be easily obtained as the zero of the function

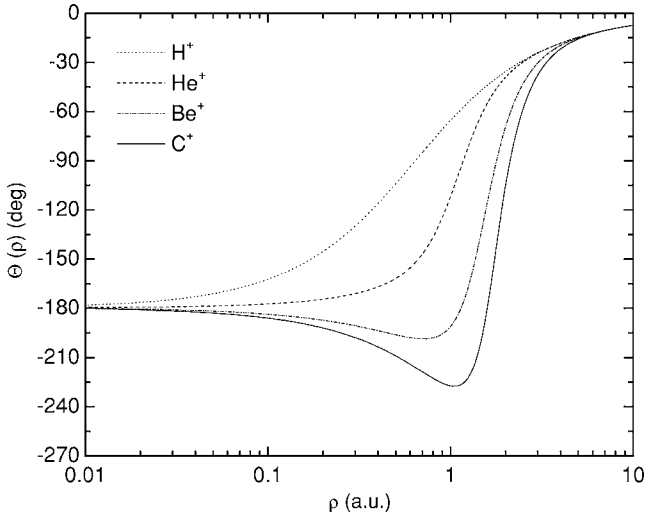

FIG. 4. Deflection function as a function of the impact parameter for electron scattering by partially stripped ions. Theories: dotted line, H^+; dashed line, He^+; dot-dashed line, Be^+; solid line, C^+. The projectile velocity is v_P=0.316 a.u.

$$\left(E - V_P(r) - \frac{l^2}{2mr^2}\right) \tag{7}$$

where $\boldsymbol{l}=m\mathbf{r}_0\times\mathbf{v}_{emis}$. The corresponding polar angle α_{min} is obtained from

$$\alpha_{min} = \pi + \phi \tag{8}$$

where ϕ is the angle between the closest approach radius vector $\mathbf{r}_{min}$ and the asymptote:

$$\phi = \int_{r_{min}}^{\infty} dr \frac{l}{mr^2}\left[\frac{2}{m}\left(E - V_P(r) - \frac{l^2}{2mr^2}\right)\right]^{-1/2}. \tag{9}$$

The polar angle at the emission instant α_0 is obtained as

$$\alpha_0 = \int_{r_0}^{\infty} dr \frac{l}{mr^2}\left[\frac{2}{m}\left(E - V_P(r) - \frac{l^2}{2mr^2}\right)\right]^{-1/2} \tag{10}$$

where we define the angle between $\mathbf{r}_{min}$ and $\mathbf{r}_0$ as $\gamma=|\alpha_0 - \alpha_{min}|$.

We assume the orbit to take place in the z, x plane. The asymptotic angle Θ is then binned, according to the values given by the components z, x of the emission velocity vector $\mathbf{v}_{emis}$:

$$(\mathbf{v}_{emis})_z > 0, \quad (\mathbf{v}_{emis})_x > 0, \quad \Theta = \pi - (\phi + \gamma),$$

$$(\mathbf{v}_{emis})_z > 0, \quad (\mathbf{v}_{emis})_x < 0, \quad \gamma + \phi < \pi, \quad \Theta = \pi + (\phi + \gamma),$$

$$(\mathbf{v}_{emis})_z > 0, \quad (\mathbf{v}_{emis})_x < 0, \quad \gamma + \phi > \pi, \quad \Theta = (\phi + \gamma) - \pi,$$

$$(\mathbf{v}_{emis})_z < 0, \quad (\mathbf{v}_{emis})_x > 0, \quad \Theta = \pi - (\phi - \gamma),$$

$$(\mathbf{v}_{emis})_z < 0, \quad (\mathbf{v}_{emis})_x < 0, \quad \Theta = \pi + (\phi - \gamma). \tag{11}$$

By so doing, we obtain the asymptotic velocity vector of an emitted electron in the projectile frame. Correspondingly, to express this vector in the target frame of reference, we simply need to add the projectile velocity vector.

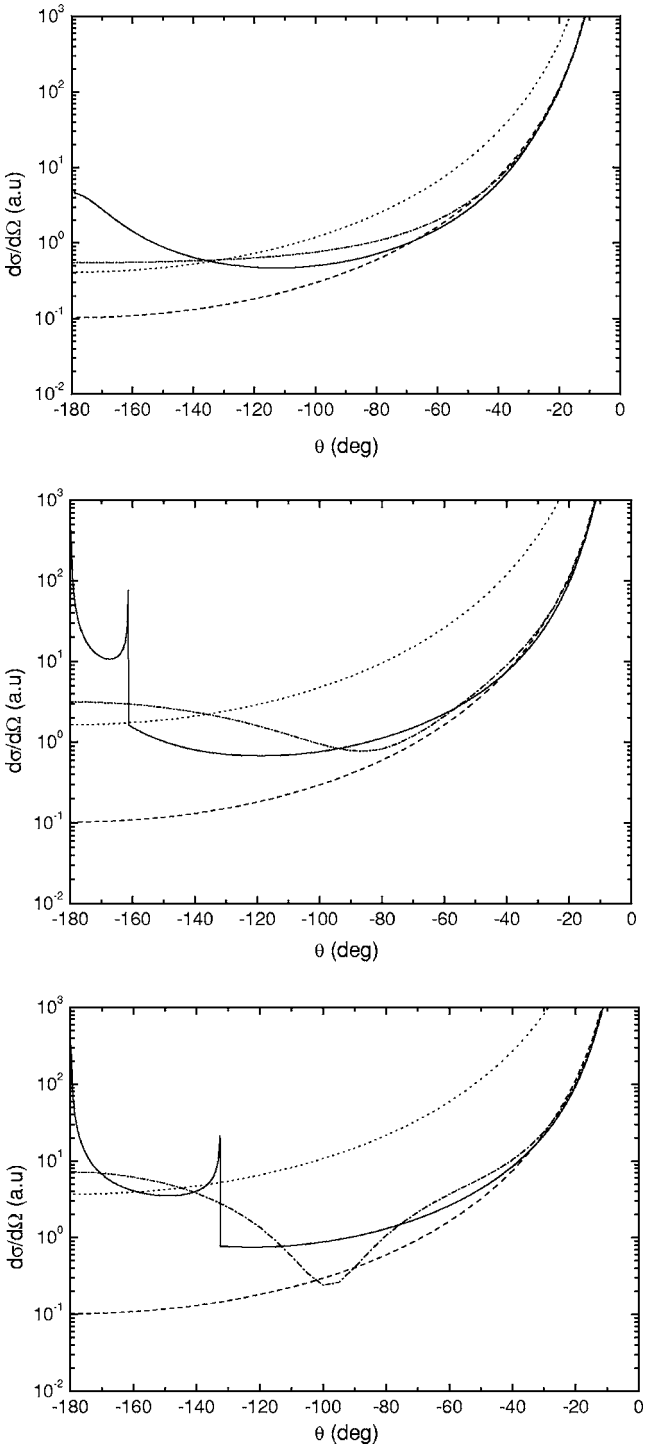

FIG. 5. Classical and quantum-mechanical elastic scattering cross sections for the different partially stripped projectiles and v_P =0.316 a.u. Theories: solid line, CEDCS; dotted line, asymptotic charge Coulomb QEDCS; dashed line, nuclear charge Coulomb QEDCS; dot-dashed line, full QEDCS as given by Eq. (14).

Using the velocity and distance distributions, it is possible to build the electron distribution in the velocity space of the electron considered in the emitter frame, as shown in Figs. 1 and 2. Here, a total of 25 000 electrons have been followed

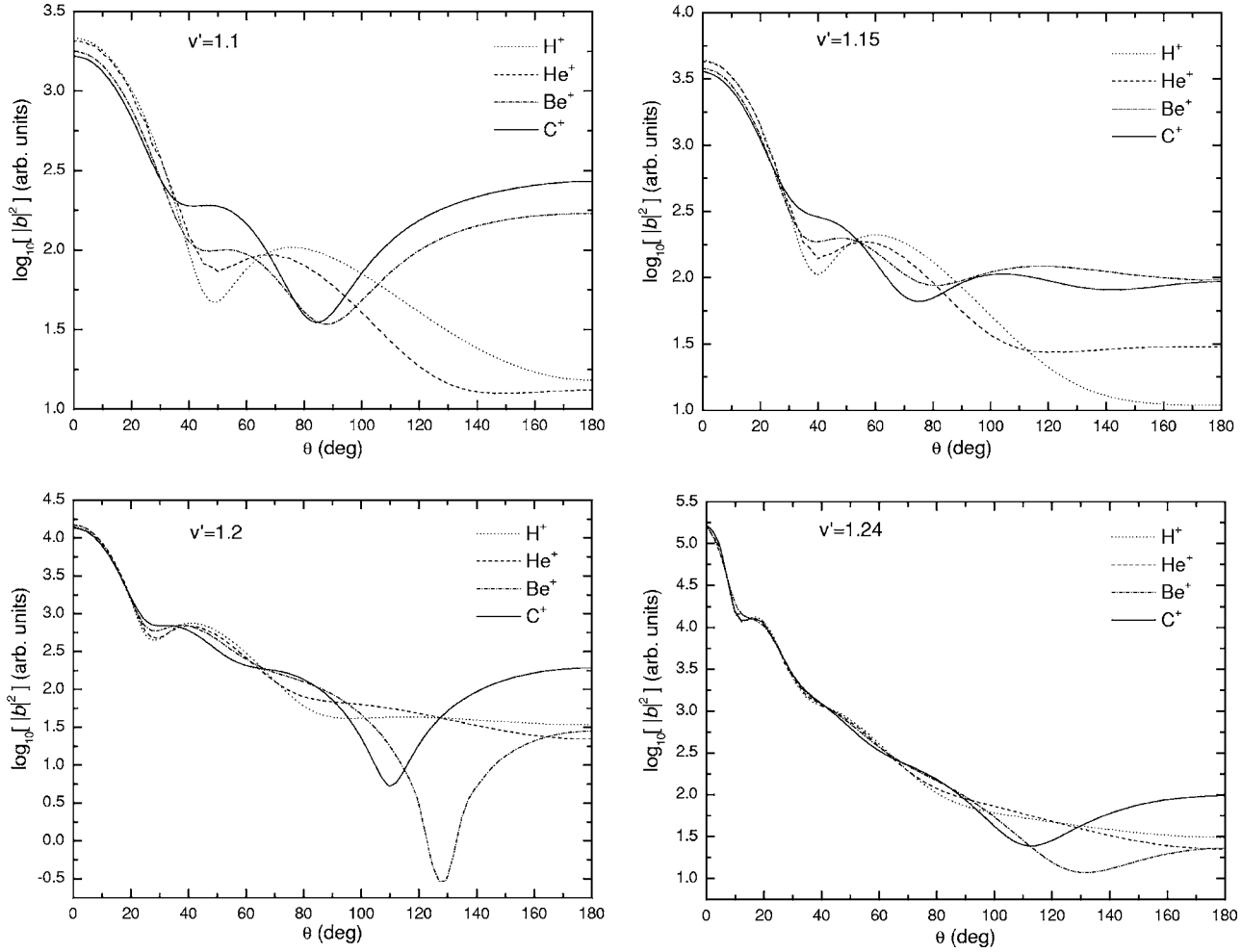

FIG. 6. Angular profile of $\log_{10}(|b_{PS}|^2)$ for different emitted electron-projectile velocities seen from the projectile frame. The impact velocity of the ions is 0.316 a.u. Theories, dotted line, H^+; dashed line, He^+; dot-dashed line, Be^+; solid line, C^+.

for the $2s^2(^1S)$ autoionizing state of He, where their velocities and projectile distances were sorted according to the above distributions. Three different projectile velocities have been considered (0.316, 1, and 1.8 a.u.) for H^+ and He^+ (Fig. 1) and Be^+ and C^+ projectiles (Fig. 2). These velocities correspond to 2.5, 25, and 80 keV/amu. The lowest velocity (0.316 a.u.) was selected since it represents a 10 keV impact energy for He^+, an energy where several experiments have been performed [6,10].

Two structures are clearly visible in the figures: the autoionization and the binary rings. The autoionization ring is already present in the photon impact case and in the present analysis represents electrons that are not significantly deflected by the projectile. On the other hand, the binary ring is a typical signature of the postcollisional interaction of electrons which pass close to the projectile and are strongly deflected. The energy change of the heavy projectile is negligible compared to its initial energy. As a consequence the electrons form a binary ring structure centered about $\mathbf{v}_P$. In the cases considered in Figs. 1(a) and 1(b) and Figs. 2(a) and 2(b), the initial electron velocity derived from the autoionization process is greater than the projectile's and the secondary binary rings are clearly visible. In Figs. 1(c) and 2(c), however, the projectile velocity is greater than that of the autoionization electrons, so a binary ring is not allowed but the electrons are pulled in the forward direction out of the autoionization ring. This is also evident in the quantum treatment, where the CDW theory evaluated in similar situations shows a minimum of intensity on the autoionization ring [20].

For large projectile velocities, most of the electrons are emitted when the projectile is already far from the target. This implies that only electrons emitted at very small forward angles, which are a minor fraction of the total emitted, can penetrate the electron shells of the projectile and be influenced by the non-Coulomb part of the interaction potential. As a result, little difference can be expected between a partially stripped projectile and a fully stripped ion of the same charge. This is the situation shown in Figs. 1(c) and 2(c), where the electron distribution is similar for all projectiles.

As the impinging energy decreases [Figs. 1(a), 1(b), 2(a), and 2(b)], the electronic distribution corresponding to the partially stripped projectile exhibits a larger fraction of backscattering. Now the electrons are created when the projectile is close to the target so that the non-Coulomb part of the electron-projectile potential strongly influences their trajec-

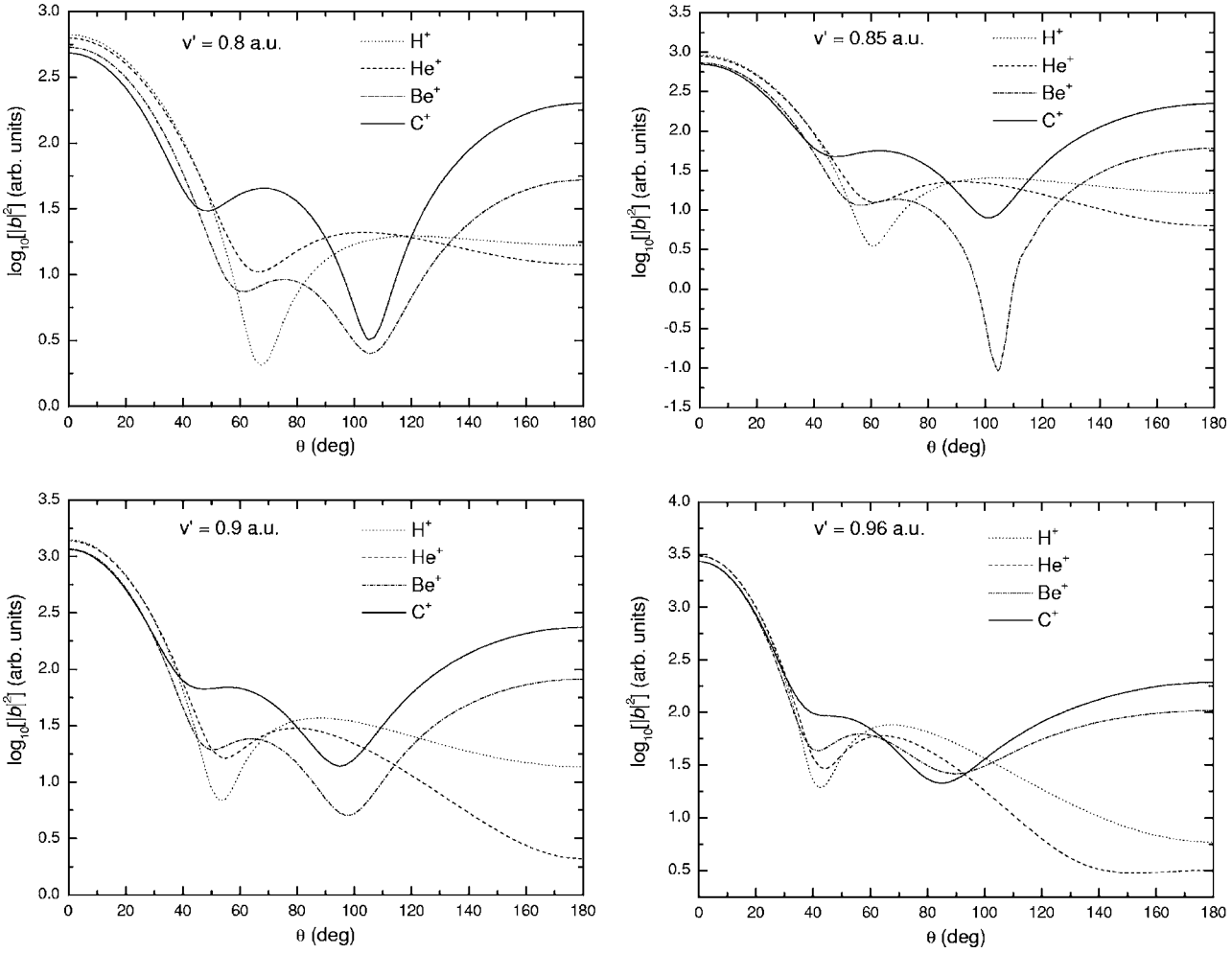

FIG. 7. Angular profile of $\log_{10}(|b_{PS}|^2)$ for different emitted electron-projectile velocities seen from the projectile frame. The impact velocity of the ions is 0.5 a.u. Theories: dotted line, H^+; dashed line, He^+; dot-dashed line, Be^+; solid line, C^+.

tories. This result becomes more evident for small differences between the emitted electron and the receding projectile velocities. Even He^+ projectiles display an angular band of strongly perturbed electrons on the binary ring close to 180° in the projectile frame. For Be^+ and C^+ projectiles this angular band extends to smaller angles in the projectile frame so that the increase of electrons emitted in the backward direction becomes clearly visible. Furthermore, for these partially stripped ions, it can be seen that this band has a sharp cutoff rather than a smooth transition.

We present histograms corresponding to the binary ring profile after sorting 5×10^6 electrons for the projectiles used above at 0.316 a.u. as seen from the projectile frame (Fig. 3). Here, the electrons are collected at relative velocities between the projectile and the electron of 1.224 to 1.2486 a.u. For H^+ projectiles, a smoothly decreasing structure is obtained which peaks at 0°. The latter peak is known as the focusing peak and appears on the binary ring and centered in the forward direction [5,6,10]. It has been associated with a forward glory effect [15,21]. Since electrons are emitted with different angles and initial distances from the projectile, an angular profile is obtained. Another important fact is that since we are considering a finite number of electrons, a maximum is obtained in the forward direction instead of a divergence. For clothed projectiles we find a sudden increase of counts in the backward direction starting at well-defined angles as was already inferred from Fig. 2. In order to explain this feature we present the deflection function for a parallel electron beam as a function of the impact parameter ρ,

$$\Theta(\rho) = \pi - 2\rho\int_{r_{min}}^{\infty}\frac{dr}{r^2}\left(1-\frac{V_P(r)}{E}-\frac{\rho^2}{r^2}\right)^{-1/2}, \qquad (12)$$

from which one obtains the classical elastic differential cross section (CEDCS)

$$\frac{d\sigma_{class}}{d\Omega} = \frac{1}{\sin\theta}\sum_i \rho_i\left|\frac{d\rho_i}{d\Theta(\rho)}\right|. \qquad (13)$$

Here i indexes the branches of the deflection function and the sum extends over all impact parameters that lead to scattering to a single angle.

In Fig. 4 the deflection function $\Theta(\rho)$ is presented for the same projectiles and the relative electron-projectile velocity used in Fig. 3. It can be seen that the deflection function

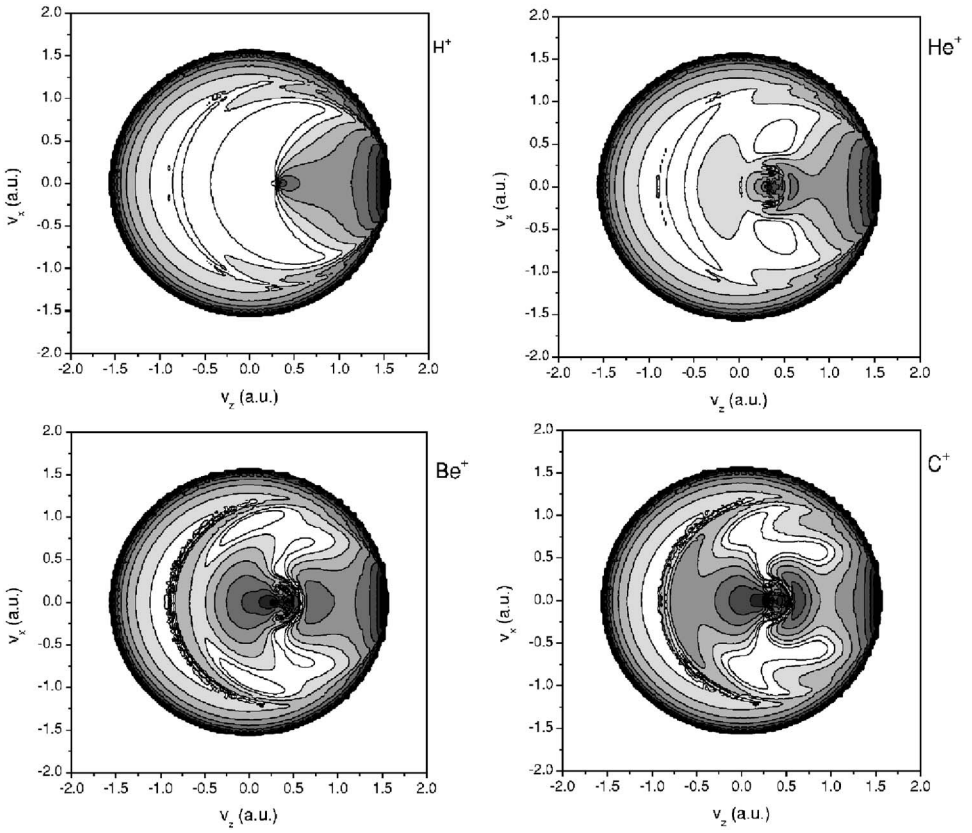

FIG. 8. Contour plot of $\log_{10}(|b_{PS}|^2)$ in velocity space for the partially stripped ions considered and $v_P=0.316$ a.u. The gray scale is selected such that darker tonalities correspond to the higher structures.

clearly exceeds 180° for Be^+ and C^+ and displays a minimum, which is denoted as the *rainbow angle*. It is in this position where the CEDCS diverges since $d\rho_i/d\Theta(\rho)\to\infty$. Since the curve for the pure Coulomb projectile clearly does not exceed 180°, it can be stated that the observed behavior can only be obtained by means of clothed ion impact. Similarly, electrons impinging with impact parameters larger than 6 or 7 a.u. have the same deflection function and their interaction with the scattering center can be considered pure Coulombic with an intensity given by the asymptotic unit charge.

III. THE QUANTUM PROBLEM

The quantum-mechanical counterpart of Eq. (13) is given by the squared modulus of the scattering amplitude which for a non-Coulomb potential reads [22]

$$f_m = f_C(\theta) + f_{nC}(\theta),$$
$$f_{nC}(\theta) = \sum_{l=0}^{\infty} \frac{1}{v'}(2l+1)e^{i(2\eta_l+\delta_l)} \sin\delta_l P_l(\cos\theta), \tag{14}$$

where we denote by v' the electron-projectile relative velocity, $\eta_l=\arg[\Gamma(1+l-iZ_p/v')]$ is the Coulomb phase shift of the l partial wave, and δ_l is the non-Coulomb-part phase shift and can be obtained by matching the logarithmic derivative of the inner and outward wave functions in the asymptotic region. The Coulomb scattering amplitude $f_C(\theta)$ is given by

$$f_C(\theta) = \frac{1}{i}\frac{\Gamma(1-iZ_p/v')}{\Gamma(iZ_p/v')}\frac{e^{i(Z_p/v')\ln[(1-\cos\theta)/2]}}{v'(1-\cos\theta)} \tag{15}$$

where $P_l(\cos\theta)$ represents the lth-order Legendre polynomial [23].

In Fig. 5 we show the CEDCS, as well as the quantum scattering amplitudes (QEDCSs) for fully and partially stripped projectiles. It can be seen that for small angles the CEDCS, $|f_m|^2$, and $|f_C^{Z=1}|^2$ are all very similar in shape and magnitude. As the scattering angle increases, the classical description displays a clear classical rainbow. For He^+ projectiles, both classical and quantum-mechanical scattering cross sections show a smooth increase as the angle tends to 180° compared with the Coulombic $Z=1$ case. For Be^+ and C^+ a clear rainbow angle appears at about 161.5° and 132.6°, respectively. In the quantum-mechanical description, an interference between the Coulomb and the non-Coulomb parts leads to a dip around 86° and 100° for Be^+ and C^+, respectively. It is in this sense that we can state that the histograms in Fig. 3 show that for low-energy clothed ions, rainbow scattering is evidenced. The rainbow angular positions in the histograms and the classical cross sections shown in Fig. 4 are in excellent agreement, giving support to our conclusion. Furthermore, the agreement in rainbow angle positions justifies the approximation that CDCSs obtained for projectile scattering assuming a parallel electron beam closely represent those obtained for electrons emitted isotropically from the target during the autoionization event.

Since for the autoionization process the binary ring profile is not only determined by the scattering amplitude f_m we

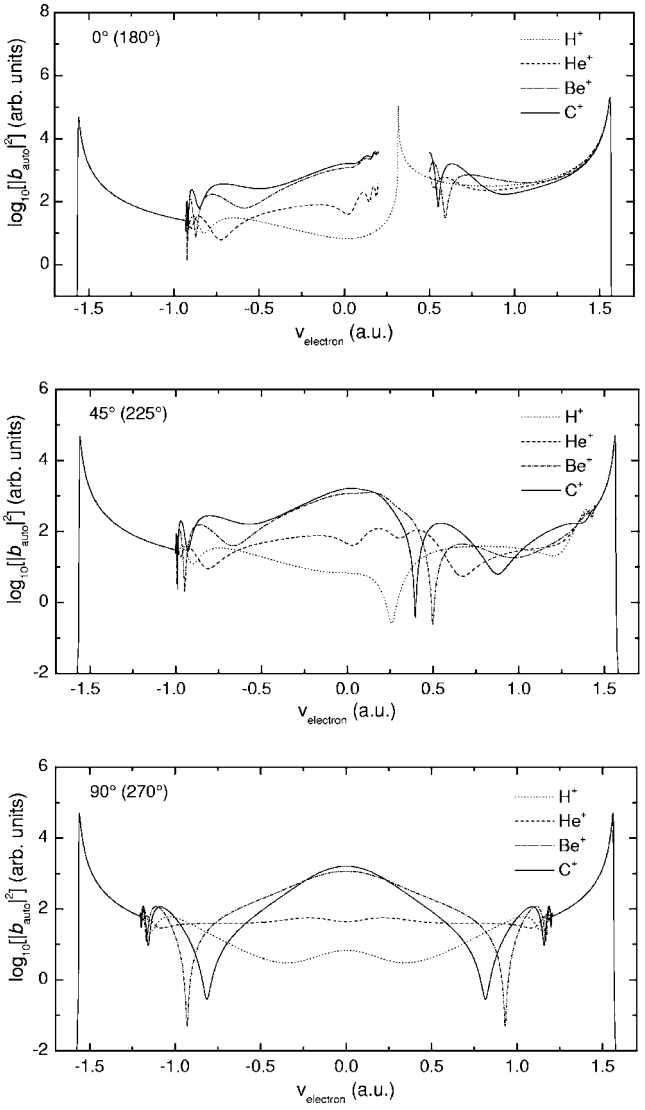

FIG. 9. Velocity profile of $\log_{10}(|b_{PS}|^2)$ for selected cuts of the velcity space: $\theta_{emitter}$=(a) 0°(180°), (b) 45°(225°), and (c) 90°(270°).

now propose a generalization of the CDW model of Barrachina-Macek that includes in the transition amplitude the information of a partially stripped ion.

The autoionization transition amplitude derived from the time-dependent perturbation theory can be expressed as [19]

$$b(t) = \int_0^t dt\, e^{i(E-E_0)t' - (\Gamma/2)t'} t'^{iZ_p/v_P} \left\langle \Psi_f^- \left| \frac{1}{r_{12}} \right| \Phi_i \right\rangle \quad (16)$$

where Ψ_f^- is the final-state wave function, Φ_i the initial-state wave function, and $1/r_{12}$ the electronic repulsion between the two excited electrons. Barrachina and Macek proposed [5] the CDW approximation, which utilizes a distorted wave in order to represent the emitted electron-receding projectile interaction,

$$\Psi_f^- \approx \Psi^-(\mathbf{r})\Gamma(1+iZ_p/v')e^{\pi Z_p/2v'}\ {}_1F_1[-iZ_p/v';1; -i[v'|\mathbf{r}-\mathbf{v}_P t| + \mathbf{v}'\cdot(\mathbf{r}-\mathbf{v}_P t)]] \quad (17)$$

where $\mathbf{r}$ is the emitted electron-target radius. Since the integrand of the matrix element $\langle \Psi_f^- | 1/r_{12} | \Phi_i \rangle$ is strongly confined to the target nucleus a peaking approximation can be performed, leading to the simplified expression

$$b_{BM} = A_0\Gamma(1-iZ_p/v') \times e^{\pi Z_p/2v'} \int_0^\infty dt\, e^{i(E-E_0)t' - (\Gamma/2)t'} \times t'^{iZ_p/v_P}\ {}_1F_1[iZ_p/v';1;i(v'v_P t - \mathbf{v}'\cdot\mathbf{v}_P t)]. \quad (18)$$

This expression separates the postcollisional interaction from a target-dependent factor A_0 and leads to an analytical expression for the transition amplitude since the integral can be solved using standard techniques [24],

$$b_{BM} = A_0\Gamma(1-iZ_p/v')\Gamma(1+iZ_p/v_P)e^{-\pi Z_p/2v_P(1-v_P/v')}(E-E_0 + i\Gamma/2)^{-1-iZ_p/v_P}\,{}_2F_1\left(i\frac{Z_p}{v'};1+i\frac{Z_p}{v_P};1;-\frac{v_P v' - \mathbf{v}_P\cdot\mathbf{v}'}{E-E_0+i\Gamma/2}\right). \quad (19)$$

This separability allows a straightforward extension of the CDW model to more complex systems as has been shown in the analysis of the Ne K-$L_{2,3}L_{2,3}$ ($^1D_2$) Auger line by Víkor *et al.* [25].

For partially stripped ions, however, a full solution requires the numerical evaluation of the radial equation for a central potential out to large distances since the integral converging factor $\Gamma/2$ is target dependent and usually rather small. In order to give a qualitative description of the different features involved for clothed ion impact, we present the following approximation which keeps the analyticity that is so useful in the CDW model:

$$\left\langle \Psi_f^- \left| \frac{1}{r_{12}} \right| \Phi_i \right\rangle \approx A_0\left(\Gamma(1-iZ_p/v')e^{\pi Z_p/2v'} \times {}_1F_1[iZ_p/v';1;i(v'v_P - \mathbf{v}'\cdot\mathbf{v}_P)t] + \frac{e^{i(v_P v' - \mathbf{v}_P\cdot\mathbf{v}')t}}{v_P t} f_{nC}(\theta)e^{i(Z_p/v')\ln(2v_P v' t)} \right). \quad (20)$$

This wave function provides the correct asymptotic limit of the exact emitted electron-projectile wave function by including the non-Coulomb part of the scattering amplitude. The additional term to the CDW model can now be easily integrated in time to yield the amplitude,

$$b_{PS} = b_{BM} + A_0\frac{1}{v_P}(2v'v_P)^{iZ_p/v'}\left(\frac{\Gamma}{2} - i(E-E_0+v'v_P - \mathbf{v}'\cdot\mathbf{v}_P)\right)^{-i(Z_p/v_P+Z_p/v')}\Gamma(i(Z_p/v_P+Z_p/v'))f_{nC}(\theta). \quad (21)$$

In Fig. 6 we show the angular squared amplitude profiles from the present model for the different projectiles along with the Barrachina-Macek model for a H^+ projectile in the projectile frame for v_P=0.316 a.u. The δ_l phases necessary to calculate $f_{nC}(\theta)$ were obtained from Salvat's code [26].

Relative velocities $v'=1.1$, 1.15, 1.2, and 1.24 a.u. are considered. It is observed that major differences are obtained among the theories. For the lowest relative velocity, Be^+ and C^+ projectiles clearly give an enhancement in the backward direction. Furthermore, the angular profile is drastically changed compared to the $Z=1$ Coulombic case. The He^+ projectile, on the other hand, gives a description closer to the Coulombic case for small angles but departs at large angles. For $v'=1.15$ a.u. similar comments can be made, plus that now the electronic emission for the partially stripped ions dominates the Coulombic one for the larger angles. For the last two velocities considered, strong dips become evident for the two heavier projectiles and the Coulombic case leads to a slightly larger emission in the 180° region compared to the He^+ and Be^+ projectiles. In Fig. 7 the projectile velocity $v_P=0.5$ a.u. is considered and relative velocities $v'=0.8$, 0.85, 0.9, and 0.96 a.u. are shown. It can be seen that in all cases, the Be^+ and C^+ projectiles lead to an enhancement in the backward emission.

In order to elucidate these trends in Fig. 8 we display contour plots for $\log_{10}(|b_{PS}|^2)$ in velocity space for $v_P=0.316$ a.u. in the emitter frame. It can be seen that the inner region to the binary ring is strongly affected by the non-Coulomb nature of the projectile and that a clear enhancement in the backward region of the binary ring is evidenced compared to the proton impact case. The above results are consistent with the classical electron angular distribution displayed in velocity space in the preceding section. The increase of counts in the inner region of the binary ring compared to the proton impact case is clearly visible for all the partially stripped ions in Figs. 1(a) and 2(a) and can be associated with the backward emission enhancement shown in Fig. 8.

In Fig. 9 we show the profiles of $\log_{10}(|b_{PS}|^2)$ in velocity space in the emitter frame for the planes defined by $\theta_{emitter}=0°(180°);45°(225°);90°(270°)$ for $v_P=0.316$ a.u. To avoid confussion, negative velocity values are given to the semiplanes indicated in parentheses. As was already inferred from Fig. 8, for partially stripped projectiles the inner region of the binary ring is clearly enhanced compared to the proton impact results. Outside the binary ring, all theories coincide and lead to the same description of the autoionization peak. In Fig. 9(a), curves for the partially stripped ions have been omitted in the region where the emitted electron velocity is very close to the projectile velocity since a strong oscillatory behavior is observed possibly as consequence of unphysical interference between the Coulomb and non-Coulomb parts of the wave function. In Fig. 9, we observe no variation between the CDW and the present model on the autoionization ring. This implies that only the electrons that pass in front of the projectile are subject to the non-Coulomb part of the interaction.

IV. CONCLUSIONS

In this work, we have considered the autoionization of He induced by partially stripped ion impact. Electron emission by target autoionization has been modeled by giving a profile in the initial velocity for the autoionizing electron as well as a probabilistic weight for the emission at different projectile distances. The present analysis has been restricted to the postcollisional interaction approach where the emitted electrons only interact with the projectile Coulomb center. A complete treatment of the problem would include the emitter Coulomb field.

The final electron distributions in velocity space have been obtained using classical trajectories and statistical initial conditions. Different partially stripped projectiles have been considered and as a result an increase in the electronic emission in the backward direction in the projectile frame, associated with a rainbow effect present only for clothed ion impact has been obtained. Furthermore, the quantum-mechanical and classical scattering cross sections for a parallel beam have been obtained and compared with the classical simulation in order to explain the marked differences from the Coulombic case.

A generalization of the CDW model has been proposed in order to obtain a quantum-mechanical description of the autoionization process induced by clothed ion impact. The present model considers an approximate wave function which gives a correct asymptotic description of the emitted electron-receding projectile interaction. As a result, a clear enhancement of the inner structure to the binary ring and major differences in the angular profiles were obtained compared to the pure Coulombic case. The present quantum model leads to results which are consistent with their classical analogues.

The present model will not give a proper representation of the electrons which are emitted in the forward direction with velocities very close to that of the projectile. Further studies are being carried out in order to give a more precise description of the emitted electron–partially-stripped-projectile interaction at all times.

ACKNOWLEDGMENTS

This work has been supported by the Office of Fusion Energy Sciences, DOE. We would like to thank Dr. J. Fiol for a critical reading of the manuscript.

[1] P. Auger, J. Phys. Radium **6**, 205 (1925).
[2] R. B. Barker, H. W. Berry, Phys. Rev. **151**, 14 (1966).
[3] A. Z. Devdariani, V. N. Ostrovskii, and Yu. N. Sebayakin, Sov. Phys. JETP **46**, 215 (1977).
[4] P. van der Straten and R. Morgenstern, J. Phys. B **19**, 1361 (1986).
[5] R. O. Barrachina and J. H. Macek, J. Phys. B **22**, 2151 (1989).
[6] J. K. Swenson, C. C. Havener, N. Stolterfoht, K. Sommer, and F. W. Meyer, Phys. Rev. Lett. **63**, 35 (1989).
[7] J. E. Miraglia and J. Macek, Phys. Rev. A **42**, 3971 (1990).
[8] I. L. Cordrey and J. H. Macek, Phys. Rev. A **48**, 1264 (1993).
[9] S. Otranto, C. R. Garibotti, F. D. Colavecchia, and G. Gasaneo,

Phys. Rev. A **63**, 022713 (2001).
[10] J. K. Swenson, J. Burgdörfer, F. W. Meyer, C. C. Havener, D. C. Gregory, and N. Stolterfoht, Phys. Rev. Lett. **66**, 417 (1991).
[11] I. Samengo, R. G. Pregliasco, and R. O. Barrachina, J. Phys. B **32**, 1971 (1999).
[12] Sh. D. Kunikeev and V. S. Senashenko, J. Exp. Theor. Phys. **82**, 839 (1996).
[13] C. O. Reinhold, D. R. Schultz, R. E. Olson, C. Kelbch, R. Koch, and H. Schmidt-Böcking, Phys. Rev. Lett. **66**, 1842 (1991).
[14] D. R. Schultz and R. E. Olson, J. Phys. B **24**, 3409 (1991).
[15] K. W. Ford and J. A. Wheeler, Ann. Phys. (N.Y.) **7**, 259 (1959).
[16] S. Otranto and G. Gasaneo, Phys. Scr. **70**, 251 (2004).
[17] R. H. Garvey, C. H. Jackman, and A. E. S. Green, Phys. Rev. A **12**, 1144 (1975).
[18] A. E. S. Green, D. L. Sellin, and A. S. Zachor, Phys. Rev. **184**, 1 (1969).
[19] C. Cohen-Tannoudji, B. Diu, and F. Laloë, *Quantum Mechanics* (John Wiley & Sons, New York, 1977), Vol. II.
[20] R. Della Picca, R. O. Barrachina, and M. Zitnik, in the *XXIII International Conference on the Physics of Electronic and Atomic Collisions, Stockholm, Sweden, 2003*.
[21] R. O. Barrachina, Nucl. Instrum. Methods Phys. Res. B **132**, 288 (1997).
[22] L. Schiff, *Quantum Mechanics* (McGraw-Hill, New York, 1955).
[23] *Handbook of Mathematical Functions*, Natl. Bur. Stand. Appl. Math. Ser. No. 55, edited by M. Abramowitz and A. Stegun (U.S. GPO, Washington, DC, 1964).
[24] I. S. Gradshteyn and I. M. Ryzhik, *Tables of Integrals, Series and Products* (Academic, London, 1965).
[25] Gy. Víkor, S. Ricz, B. Sulik, L. Tóth, A. Kövér, and J. Végh, J. Phys. B **29**, L787 (1996).
[26] F. Salvat, J. M. Fernández-Varea, and W. Williamson, Jr., Comput. Phys. Commun. **90**, 151 (1995).